

Ab initio approach to the optimization of qubit manipulationCarlos F. Destefani,^{1,*} Chris McDonald,^{1,†} Ramin M. Abolfath,^{2,3} Pawel Hawrylak,² and Thomas Brabec¹¹*Department of Physics and Center for Photonics Research, University of Ottawa, Ottawa, Ontario, Canada K1N 6N5*²*Institute for Microstructural Sciences, National Research Council, Ottawa, Ontario, Canada K1A 0R6*³*Department of Radiation Oncology, Southwestern Medical Center, University of Texas, Dallas, Texas 75390, USA*

(Received 21 August 2008; published 31 October 2008)

We investigate the multiconfiguration time-dependent Hartree-Fock approach and show that it relaxes computational requirements and makes accurate modeling of few-electron dynamics in nanodevices computationally feasible. The method is applied to the optimization of the manipulation of a two-electron spin-based coded qubit in a double quantum dot and is successfully tested against direct integration of the multidimensional time-dependent Schrödinger equation. Our investigation presents a basis for the *ab initio* optimization of few-qubit operations, which is prohibitively difficult to do with other numerical methods.

DOI: 10.1103/PhysRevB.78.165331

PACS number(s): 73.21.La, 85.35.Be, 03.67.Pp

I. INTRODUCTION

Ideally, a qubit is an isolated two-level system, which can be controlled and manipulated for an unlimited time. In practice, qubits are embedded in the spectrum of a host system, which is surrounded by an environment. Leakage, i.e., probability of the system being out of the qubit subspace, to the host spectrum and to the environment leads to information loss and compromises the qubit fidelity. This determines the maximum time, τ_q , over which quantum computation can be performed.

Leakage to the host spectrum can be kept small by performing qubit operations close to the adiabatic limit. However, this limits the time required for one operation to $\tau \gg 1/\Delta^2$, where Δ is the energy difference between the qubit subspace and the next closest level of the host spectrum. As a result, the number of maximum qubit operations is $N_m \propto \tau_q/\tau$. A lot of effort has been put into maximizing N_m by minimizing both the leakages to the host spectrum¹ and to the environment.²

Our work focuses on controlling the coupling between qubit and host spectrum. In the absence of an environment, N_m is maximized by shortening τ and by minimizing the leakage to the host system, L_1 . When τ is reduced, the qubit manipulation takes place in the nonadiabatic regime; i.e., an increasingly broader band of the host spectrum is populated. In order to regain the leaked population at the end of the manipulation, optimum coherent control theory has to be used.³

Usually, qubit dynamics are modeled using various degrees of approximations based on a reduced Hilbert space, such as by a Hund-Mulliken picture,⁴ by a multilevel expansion based on adiabatic eigenfunctions,⁵ or by reducing the spatial dimensions per electron to one-dimensional (1D).⁶ Whereas these approximations are sufficient for a qualitative analysis of the dynamics, it is often not clear how close they are to the exact result.

For quantum computation to work, a leakage per operation of $L_1 < 10^{-4}$ is required.⁷ As a result, computational approaches with corresponding accuracy are required to quantitatively assess the effectiveness and limits of coherent control methods. To date, little work exists in this direction,

and quantitative data of N_m is scarce. The main reason for this shortcoming is a lack of efficient methods that can integrate the multidimensional time-dependent Schrödinger equation (TDSE) numerically. Exact calculation of the multidimensional wave function is prohibitively difficult, as computational demands increase exponentially with the number of qubits.

We report here progress on this challenge. We investigate the multiconfiguration time-dependent Hartree-Fock (MCTDHF) approach^{8–10} and show that it relaxes computational requirements and opens the door to accurate (10^{-4} – 10^{-5}) modeling and optimization of few-electron dynamics in nanodevices and in a broad range of other host systems.

The MCTDHF approach builds on the time-dependent configuration-interaction (TDCI) method.¹¹ We find that TDCI is in general not ideally suited for modeling few-electron qubit dynamics for two reasons. (i) In the nonadiabatic limit, where a significant fraction of the host spectrum becomes populated, convergence to accuracies better than 10^{-2} is extremely slow, and therefore difficult to achieve. (ii) As the complexity of the spectrum increases rapidly with the number of qubits, the required number of configurations quickly becomes unmanageable. MCTDHF relaxes these constraints by optimizing the basis functions in addition to the TDCI coefficients, reducing the size of the required Hilbert space.

In this paper, MCTDHF is tested and used to optimize the initialization of two-electron spin-based coded qubits in a two-dimensional (2D) double quantum dot (DQD).^{12–19} MCTDHF is successfully tested against direct integration of the four-dimensional (4D) TDSE. Optimization is performed in the strongly nonadiabatic limit on a simple class of potential ramps, consisting of three linear ramps with variable gradients.

II. QUBIT SUBSPACE

Figure 1(a) shows a schematic of the two-electron DQD potential, given by $V(\mathbf{r}, t) = V_l(\mathbf{r}, t) + V_b(\mathbf{r}, t) + V_r(\mathbf{r}, t)$. The potentials of the left, right dot and of the barrier ($i=l, r, b$) are given by $V_i(\mathbf{r}, t) = W_i(t)U_i(\mathbf{r})$, where $U_i(\mathbf{r}) = \exp[-(\mathbf{r} - \mathbf{d}_i)^2/\Delta_i^2]$; the left, right dot is centered at $\mathbf{d}_{l,r} = (\mp d, 0)$,

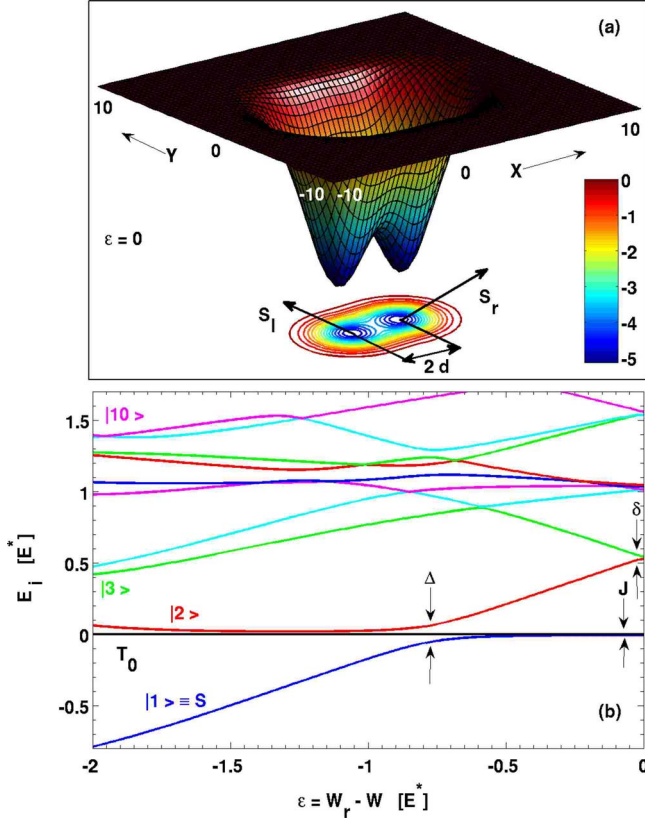


FIG. 1. (Color online) Panel (a): schematic of the 2D symmetric DQD potential profile with one electron in each dot, $S_{l(r)}$; the grid lines depict the numerical grid used in our simulations: 64 points per dimension in a box ranging from -10 to 10 ; the dots are centered at $(x,y)=(\pm d,0)$. The detuning between left and right dot is given by $\epsilon = W_r - W$. Panel (b): two-electron spectrum E_i as a function of ϵ for the lowest ten singlets; energy is plotted with reference to the lowest triplet T_0 . Δ , δ , and J denote, respectively, the tunneling splitting between singlets $|1\rangle \equiv S$ and $|2\rangle$, between singlets $|2\rangle$ and $|3\rangle$, and the exchange splitting between S and T_0 , which depend on ϵ and W_b ; the arrows indicate the values $J(\epsilon=0)=0.007$, $\Delta(\epsilon=-0.77)=0.116$, and $\delta(\epsilon=0)=0.017$. The triplets T_+ , T_- are not shown, as they are usually split off by an additional magnetic field, which isolates the $S_z=0$ two-level subspace formed by S and T_0 . Two-electron spectrum calculated from configuration interaction (CI) diagonalization by using the one-electron basis at each given value of ϵ .

while the barrier is located at $\mathbf{d}_b=(0,0)$. The widths and heights of the dots and the barrier are given by Δ_i and $W_i(t)$, respectively. Only the right dot potential $W_r(t)=W+\epsilon(t)$ is assumed to be biased with time, while $W_l(t)=W$ and $W_b(t)=W_b$ are held constant. The potential detuning is $\epsilon(t)=W_r(t)-W$, which is varied in the range $-2 \leq \epsilon \leq 0$. In the symmetric DQD limit, $\epsilon=0$, shown in Fig. 1(a), each dot has one-electron spin, $S_{l(r)}$; in the asymmetric limit, $\epsilon=-2$, both electrons occupy the right dot.

The DQD parameters used here are $\Delta_l=\Delta_r=2.5$, $\Delta_b=1.5$, $W=-5$, $W_b=1.5$, and $d=2$. We use effective atomic units throughout the paper; energy, size, and time are given in terms of effective Bohr radius R^* , effective Hartree energy E^* , and effective natural time T^* , which in GaAs are $R^*=9.80$ nm, $E^*=11.85$ meV, and $T^*=55.55$ fs, respectively.

The operation of a spin-based coded qubit¹⁶ in a DQD is summarized in Fig. 1(b). The qubit is encoded in the two lowest levels of the DQD spectrum, which are the singlet ground state $|1\rangle \equiv S$ and the triplet T_0 . The qubit operation is a three-stage process: (i) Initialization; after starting in the asymmetric ($\epsilon \ll 0$) singlet ground state S with left, right charge $(Q_l, Q_r)=(0, 2)$, the bias is switched off ($\epsilon \rightarrow 0$) adiabatically. This transfers the system into the ground state S of the symmetric DQD with $(1,1)$ charge configuration. (ii) Manipulation; the spin qubit is encoded in the $S-T_0$ states, and can be addressed due to the small singlet-triplet splitting J at $\epsilon=0$. (iii) Measurement; the DQD is adiabatically biased back to its initial state. By assuming spin-to-charge conversion the charge measured on the right dot can be directly related to the population of the qubit singlet state at the end of stage (ii).

The assumption that the remaining Hilbert space in Fig. 1(b) does not play a role in any of those three stages stays valid as long as the biasing occurs adiabatically. We define the adiabatic regime by the [stage (i)] initialization time τ_a for which the leakage $L_1=10^{-4}$; for the parameters used here $\tau_a \approx 600$. For nonadiabatic time scales $< \tau_a$, charge leaks to excited singlet states, compromising the gate fidelity; if some population remains in state $|2\rangle$ once the manipulation stage (ii) is reached, further leakage will happen to state $|3\rangle$ due to the smallness of the $|2\rangle$ - $|3\rangle$ splitting δ at $\epsilon=0$, and from there to higher states during the ramp-down stage (iii).

III. MULTICONFIGURATION TIME-DEPENDENT HARTREE-FOCK APPROACH

The two-electron dynamics of the spin-based coded qubit is described by the Schrödinger equation

$$i \frac{\partial}{\partial t} \Psi = H(\mathbf{r}_1, \mathbf{r}_2, t) \Psi = \left[\sum_{i=1}^2 H_1(\mathbf{r}_i, t) + H_2(\mathbf{r}_1, \mathbf{r}_2) \right] \Psi, \quad (1)$$

where the wave function is $\Psi = \Psi(\mathbf{r}_1, \mathbf{r}_2, t) \otimes |S\rangle$, $\mathbf{r}=(x,y)$ is the 2D space vector, and the spin singlet state is $|S\rangle = |\uparrow\downarrow\rangle - |\downarrow\uparrow\rangle$, which is conserved throughout our analysis. The one-electron Hamiltonian is $H_1 = T + V(\mathbf{r}, t)$, with $T = -\nabla^2/2$ the kinetic-energy operator, and the two-electron Hamiltonian is $H_2 = 1/\sqrt{(\mathbf{r}_2 - \mathbf{r}_1)^2 + a^2}$, with parameter a arising from the finite thickness of the 2D DQD (we use $a=0.5$).

Equation (1) is solved by the MCTDHF approach,⁸⁻¹⁰ which relies on the ansatz

$$\Psi(\mathbf{r}_1, \mathbf{r}_2, t) = \sum_{j_1 \neq j_2=1}^n A_{j_1 j_2}(t) \varphi_{j_1}(\mathbf{r}_1, t) \varphi_{j_2}(\mathbf{r}_2, t) |s_{j_1}\rangle |s_{j_2}\rangle. \quad (2)$$

The discussion here is confined to two electrons for the sake of simplicity. The n single-particle basis functions are characterized by a spin $s_j = \uparrow, \downarrow$ and by an orbital part φ_j . We use restricted MCTDHF with $n/2$ different orbital basis functions; the resulting number of configurations is $\binom{n}{2}$. The antisymmetry of the wave function Ψ is ensured by imposing the constraint $A_{j_1 j_2} = -A_{j_2 j_1}$ on the expansion coefficients. Both $A_{j_1 j_2}(t)$ and $\varphi_j(\mathbf{r}, t)$ are time dependent and are determined by the Dirac-Frenkel variational principle,

$$\langle \delta\Psi(t) | i \frac{\partial}{\partial t} \Psi(t) - H(t) | \Psi(t) \rangle = 0. \quad (3)$$

Performing the variation with regard to Eq. (2) yields a set of time-dependent, nonlinear coupled integrodifferential equations for $A_{j_1 j_2}(t)$ and $\varphi_j(\mathbf{r}, t)$,

$$i \frac{\partial}{\partial t} A_{j_1 j_2}(t) = \sum_{l_1 \neq l_2=1}^n H_{j_1 j_2 l_1 l_2}(t) A_{l_1 l_2}(t), \quad (4)$$

$$i \frac{\partial}{\partial t} \varphi_j(\mathbf{r}, t) = [1 - P(\mathbf{r}, t)] \sum_{k,l=1}^n R_{jlk}(\mathbf{r}, t) \varphi_k(\mathbf{r}, t), \quad (5)$$

where $R_{jlk}(\mathbf{r}, t) = \rho_{jl}^{-1}(t) \langle H \rangle_{lk}(\mathbf{r}, t)$, with $\rho_{jl}(t) = \sum_{i=1}^n A_{ji}^*(t) A_{li}(t)$ as the density matrix. Further, the projector is $P(\mathbf{r}, t) = \sum_{i=1}^n |\varphi_i(\mathbf{r}, t) \rangle \langle \varphi_i(\mathbf{r}, t)|$, the mean field is given by

$$\langle H \rangle_{lk}(\mathbf{r}, t) = \sum_{i=1}^n \langle A_{li}(t) \varphi_i(\mathbf{r}_2, t) | H(t) | A_{ki}(t) \varphi_i(\mathbf{r}_2, t) \rangle, \quad (6)$$

while the two-electron matrix elements are given by

$$H_{j_1 j_2 l_1 l_2}(t) = \langle \varphi_{j_1}(\mathbf{r}_1, t) \varphi_{j_2}(\mathbf{r}_2, t) | H(t) | \varphi_{l_1}(\mathbf{r}_1, t) \varphi_{l_2}(\mathbf{r}_2, t) \rangle. \quad (7)$$

The ground state at $t=0$ is found via imaginary time propagation. This converged set of orbitals and coefficients is then taken as the initial state in the propagation of Eqs. (4) and (5), which yields the many-particle wave function in Eq. (2) at any time instant.

We compare MCTDHF with two other approaches: (i) with TDCI, which is a special case of MCTDHF, where the basis functions are kept fixed in time, that is, $P=1$ in Eq. (5); (ii) with a direct split-step integration²⁰ of the 4D TDSE.

IV. QUBIT DYNAMICS

In the following, we first investigate the nonadiabatic²¹ dynamics of the orbital degrees of freedom in the three-stage qubit operation described above. Spin manipulation of the $S-T_0$ qubit, which occurs during stage (ii), and coupling to the environment are not regarded here. Then, MCTDHF is used to optimize L_1 for the nonadiabatic initialization pulse.

A. Convergence of MCTDHF compared with TDCI and exact approaches

In Fig. 2, we show the ground-state probability $P_1(\tau) = |\langle \Psi_1(0) | \Psi_1(\tau) \rangle|^2$, at the end ($t=\tau$) of the biasing pulse $\epsilon(t)$ shown in the inset, as a function of the number of orbitals (bottom) and configurations (top). The chosen ramping and plateau times, $t_r = t_p = 50$, reflect a worst case scenario that requires a large number of orbitals to converge the highly nonadiabatic dynamics. We have plotted the MCTDHF (circles) and TDCI (squares) results, and for comparison, the exact result from the integration of the 4D TDSE (line). For $n=50$, the difference between MCTDHF and the exact result is $\approx 3.1 \times 10^{-4}$. For all other test calculations the agreement was even better, between 10^{-4} and 10^{-5} . As a result, $n \approx 50$

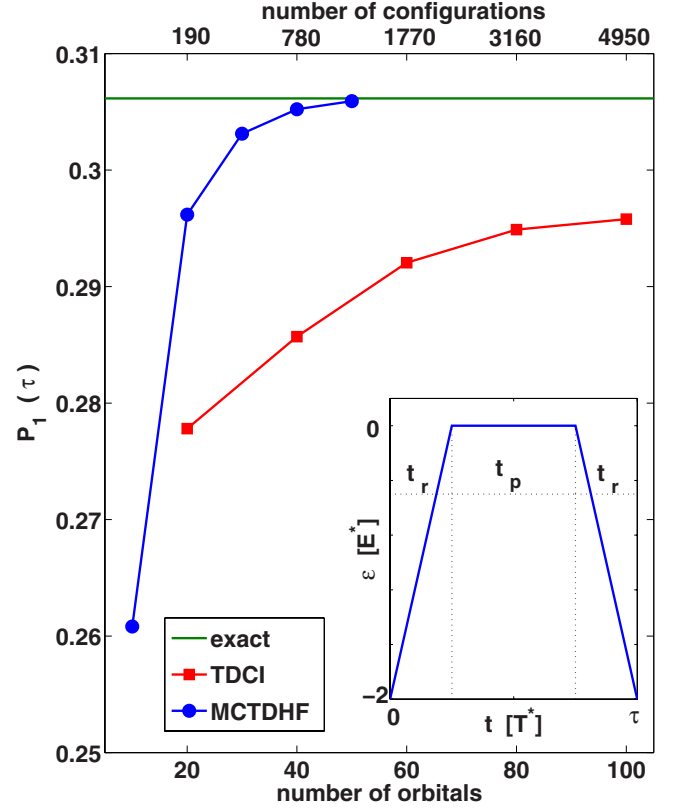


FIG. 2. (Color online) Ground-state probability $P_1(\tau)$ after a completed gate cycle (see inset, for $t_r = t_p = 50$) versus number of orbitals or configurations (bottom or upper x axis). Results from MCTDHF (TDCI) approach are shown with circles (squares), while result from the exact solution of the 4D TDSE is shown as solid line. Inset. Three-stage symmetric bias pulse applied to the right dot: ramp up (t_r) from (0,2) to (1,1) charge configuration; symmetric DQD maintained during plateau (t_p); ramp back to the initial configuration (t_r). The full cycle takes $\tau = 2t_r + t_p$.

yields the accuracy required for modeling and optimizing qubit dynamics.

On the other hand, TDCI converges much slower. Its convergence depends strongly on the chosen basis. We have tested different basis sets and found fastest convergence for the one-electron basis of the initially biased ($\epsilon = -2$) DQD. Although TDCI converges quickly to an accuracy of $\approx 1.1 \times 10^{-2}$ for $n=100$, convergence to higher accuracies is slow and requires unmanageably large basis sizes. This demonstrates the advantage of the MCTDHF basis set optimization during each time step. However, it has to be emphasized that in the adiabatic regime the convergence issues of TDCI disappear.

The computation time on a Xeon E8400 2.8 GHz single core processor is 27 h for MCTDHF ($n=50$), 15 h for TDCI ($n=100$), while the 4D exact integration takes 16 h. Although the exact approach is more efficient than MCTDHF in our test calculation, this changes for a larger number of electrons, and for a higher number of grid points (larger DQDs), as the number of points of the exact wave function grows as $(N_x N_y)^f$. Here, $N_{x(y)}$ is the number of grid points in the x (y) direction and f is the number of electrons. When N_x, N_y are doubled for $f=2$, the exact wave function in-

creases by 16, while MCTDHF ansatz increases only by a factor of 4. Further, the more favorable scaling of MCTDHF with f makes it possible to calculate few-electron dynamics.

For TDCI, the workload goes into the calculation of the time-dependent coefficients, which scales with $\binom{n}{f}$; for $n = 100$, the number of configurations for $f > 2$ electrons explodes, e.g., for $f = 5$ one has $\approx 10^8$ configurations. MCTDHF trades off a lower number of orbitals against the solution of partial differential equations for orbital optimization. For $f = 2$ the main computational effort goes into the optimization of the orbitals; even there the optimized basis gives MCTDHF a clear gain over TDCI, as Fig. 2 shows. The gain will become far more pronounced for an increasing number of electrons, where the workload shifts more toward the calculation of the configuration coefficients.

B. Nonadiabatic qubit initialization

With the validity of the MCTDHF method established, we can now use it to optimize the bias pulse of Fig. 2. We focus here on the qubit initialization, which occurs during the linear ramp up. For demonstration purposes, a simple class of optimization functions is used, consisting of three linear ramps (see dotted line in Fig. 3). Optimization is done in the following way. We first solve the multilevel⁵ equations for the first ten adiabatic eigenstates of the DQD to scan the parameter space. Then, MCTDHF, in combination with the Newton algorithm, is used for finding the local maximum for P_1 .

The result is shown in Fig. 3, where P_1 is plotted as a function of time. The result for the single ramp up of Fig. 2 (dashed line) is compared with the optimized triple ramp up (solid line). The leakage $L_1 \equiv 1 - P_1$ is improved by ≈ 2 orders of magnitude, from $\approx 4.6 \times 10^{-1}$ to $\approx 1.4 \times 10^{-3}$, for the same initialization time of $t_r = 52$, which is 1 order of magnitude smaller than the adiabatic time τ_a . In order to reach the threshold of $L_1 < 10^{-4}$ required for quantum computation, L_1 has to be further improved by using a more refined set of optimization functions.²²

V. CONCLUSION

We have demonstrated that MCTDHF is capable of quantitatively describing few-electron dynamics and to predict parameters such as leakage, which are of fundamental importance for quantum computation. We believe that MCTDHF is currently the most viable approach for the analysis of the

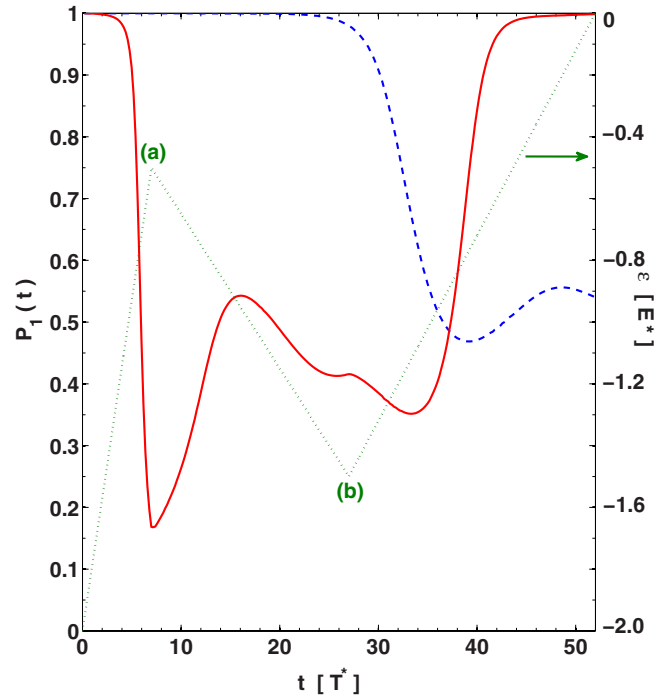


FIG. 3. (Color online) Time-evolution of ground-state probability P_1 during the qubit initialization stage for $t_r = 52$. Solid line is for the optimized triple linear ramp up, shown as dotted lines. The optimum values are $(t_a, \epsilon_a) = (7.0, -0.5)$ and $(t_b, \epsilon_b) = (27.0, -1.5)$. A similar shape can be used for the ramp-down (measurement) stage. Dashed line considers the single linear ramp up (see inset of Fig. 2).

reliability and optimization of few-qubit operations.

MCTDHF was applied to nonadiabatically accelerate spin-based coded qubit operation in a two-electron DQD. Only the orbital degrees of freedom were considered. Although coupling to the environment was not considered here, speeding up of qubit operations is a powerful way to reduce the influence of the environment since shorter operation times result in a reduced leakage per operation to the environment. The extension to include spin and coupling to the environment is straightforward and will be done in a future work.

ACKNOWLEDGMENT

R.M.A. and P.H. acknowledge partial support from Canadian Institute for Advanced Research and Quantum Works.

*carlos.destefani@uottawa.ca

†cmcd059@uottawa.ca

¹G. Burkard, D. Loss, and D. P. DiVincenzo, Phys. Rev. B **59**, 2070 (1999).

²I. A. Merkulov, A. L. Efros, and M. Rosen, Phys. Rev. B **65**, 205309 (2002).

³S. E. Sklarz and D. J. Tannor, Phys. Rev. A **66**, 053619 (2002).

⁴J. Schliemann, D. Loss, and A. H. MacDonald, Phys. Rev. B **63**,

085311 (2001).

⁵X. Hu and S. Das Sarma, Phys. Rev. A **66**, 012312 (2002).

⁶G. E. Murgida, D. A. Wisniacki, and P. I. Tamborenea, Phys. Rev. Lett. **99**, 036806 (2007).

⁷J. H. Jefferson, M. Fearn, D. L. J. Tipton, and T. P. Spiller, Phys. Rev. A **66**, 042328 (2002).

⁸M. H. Beck, A. Jäckle, G. A. Worth, and H. D. Meyer, Phys. Rep. **324**, 1 (2000).

- ⁹J. Zanghellini, M. Kitzler, T. Brabec, and A. Scrinzi, *J. Phys. B* **37**, 763 (2004).
- ¹⁰J. Caillat, J. Zanghellini, M. Kitzler, O. Koch, W. Kreuzer, and A. Scrinzi, *Phys. Rev. A* **71**, 012712 (2005).
- ¹¹L. Saalen, R. Nepstad, I. Degani, and J. P. Hansen, *Phys. Rev. Lett.* **100**, 046805 (2008).
- ¹²D. Loss and D. P. DiVincenzo, *Phys. Rev. A* **57**, 120 (1998).
- ¹³D. P. DiVincenzo, D. Bacon, J. Kempe, G. Burkard, and K. B. Whaley, *Nature (London)* **408**, 339 (2000).
- ¹⁴J. Levy, *Phys. Rev. Lett.* **89**, 147902 (2002).
- ¹⁵M. Pioro-Ladriere, M. Ciorga, J. Lapointe, P. Zawadzki, M. Korkusinski, P. Hawrylak, and A. S. Sachrajda, *Phys. Rev. Lett.* **91**, 026803 (2003).
- ¹⁶J. R. Petta, A. C. Johnson, J. M. Taylor, E. A. Laird, A. Yacoby, M. D. Lukin, C. M. Marcus, M. P. Hanson, and A. C. Gossard, *Science* **309**, 2180 (2005).
- ¹⁷F. H. L. Koppens, C. Buizert, K. J. Tielrooij, I. T. Vink, K. C. Nowack, T. Meunier, L. P. Kouwenhoven, and L. M. K. Vandersypen, *Nature (London)* **442**, 766 (2006).
- ¹⁸L. Gaudreau, S. A. Studenikin, A. S. Sachrajda, P. Zawadzki, A. Kam, J. Lapointe, M. Korkusinski, and P. Hawrylak, *Phys. Rev. Lett.* **97**, 036807 (2006).
- ¹⁹R. Hanson and G. Burkard, *Phys. Rev. Lett.* **98**, 050502 (2007).
- ²⁰A. D. Bandrauk and S. Shen, *J. Phys. A* **27**, 7147 (1994).
- ²¹K. Saito and Y. Kayanuma, *Phys. Rev. B* **70**, 201304(R) (2004).
- ²²A. Mitra, T. S. Mahesh, and A. Kumar, *J. Chem. Phys.* **128**, 124110 (2008).